Off-Center Carbon Ignition in Rapidly Rotating, Accreting Carbon-Oxygen White Dwarfs

Hideyuki Saio

Astronomical Institute, Graduate School of Science, Tohoku University, Sendai, 980-8578, Japan

saio@astr.tohoku.ac.jp

and

Ken'ichi Nomoto

Department of Astronomy, Graduate School of Science, University of Tokyo, Hongo 7-3-1, Bunkyo-ku, Tokyo 113-0033, Japan

nomoto@astron.s.u-tokyo.ac.jp

ABSTRACT

We study the effect of stellar rotation on the carbon ignition in a carbon-oxygen white dwarf accreting CO-rich matter. Including the effect of the centrifugal force of rotation, we have calculated evolutionary models up to the carbon ignition for various accretion rates. The rotation velocity at the stellar surface is set to be the Keplerian velocity. The angular velocity in the stellar interior is determined by taking into account the transport of angular momentum due to turbulent viscosity. We have found that an off-center carbon ignition occurs even when the effect of stellar rotation is included if the accretion rate is sufficiently high; the critical accretion rate for the off-center ignition is hardly changed by the effect of rotation. Rotation, however, delays the ignition; i.e., the mass coordinate of the ignition layer and the mass of the white dwarf at the ignition are larger than those for the corresponding no-rotating model. The result supports our previous conclusion that a double-white dwarf merger would not be a progenitor of a SN Ia.

Subject headings: accretion – stars: evolution – stars: rotation – supernovae: general – white dwarfs

1. Introduction

Mass accretion onto a white dwarf, which may occur in a close binary system, plays an important role in its evolution. If the accretion rate is sufficiently high, heating of the outer layers of the accreting star leads to the ignition of nuclear burning. A C-O white dwarf accretes CO-rich matter if the companion is also a C-O white dwarf (i.e., double C-O white dwarf system). Whether the carbon is ignited in the stellar center or in the envelope of an accreting C-O white dwarf is crucial for the star's fate. If the ignition occurs at the center, it leads to a SN Ia explosion. If carbon burning is ignited in the envelope, on the other hand, the flame propagates inward to the center converting the C-O white dwarf to an O-Ne-Mg white dwarf (Saio & Nomoto 1985, 1998; Timmes et al. 1994) that is expected to eventually collapse to a neutron star (Nomoto 1984, 1987; Nomoto & Kondo 1991). Nomoto & Iben (1985) and Kawai et al. (1987) have shown that carbon-ignition occurs in an outer layer if the C-O white dwarf accretes matter more rapidly than $2.7 \times 10^{-6} M_{\odot} \mathrm{y}^{-1}$.

When a double C-O white-dwarf system coalesces due to angular momentum loss by gravitational wave radiation and/or by a magnetic field, the less massive white dwarf is disrupted to become a thick disk around the more massive white dwarf (Iben & Tutukov 1984; Webbink 1984; Benz et al. 1990; Rasio & Shapiro 1995). If the thick disk is turbulent, which is likely, the timescale of viscous angular momentum transport is very short (Mochkovitch & Livio 1990) so that the more massive white dwarf is expected to accrete CO-rich matter at a rate close to the Eddington limit from the thick disk. Therefore, when a double C-O white-dwarf system coalesces, carbon burning is ignited in the envelope of the more massive white dwarf to transform it to an O-Ne-Mg white dwarf, thus preventing the occurrence of the SN Ia explosion postulated by Iben & Tutukov (1984) and Webbink (1984). In the previous investigations on the carbon ignition, however, the effect of rotation was neglected despite the fact that the accreted matter should bring angular momentum to the white dwarf. It is important to see whether the above conclusion on the fate of a double white dwarf merger is unchanged when the effect of rotation is included.

Recently, Piersanti et al. (2003a) investigated the effect of rotation on the evolution of white dwarfs that accrete CO-rich matter. They assumed that all the angular momentum associated with the accreted matter was brought into the white dwarf. They claim that the combined effects of accretion and rotation induce expansion to make the surface zone gravitationally unbound and hence suppresses further accretion in the double white dwarf merger. They argued that the above effect makes the accretion rate smaller than the critical value for the occurrence of the off-center carbon ignition, and hence the white dwarf can grow up to the Chandrasekhar mass to become a SN Ia. In addition to the above assumption Piersanti et al. (2003b) took into account the angular momentum loss via gravitational wave

radiation, and obtained an evolutionary model leading to a central carbon ignition.

In contrast to their assumption, Paczyński (1991) and Popham & Narayan (1991) had shown that when the surface rotation rate is nearly critical, angular momentum is transported from the star back to the accretion disk (see also Fujimoto (1995)) and the star can continue to accrete matter as long as matter exists around the star. This indicates that we should let matter accrete onto the white dwarf keeping the surface rotation velocity nearly critical. Those results were obtained by considering a central star at contact with a thin disk, in contrast of a thick disk expected in the case of a merging two white dwarfs. Although the physics of thick disk accretion is poorly known, we expect that the thick disk is turbulent and the angular momentum would be exchanged as fast as in a thin disk. Therefore, it is likely that the results of Paczyński (1991) and Popham & Narayan (1991) are applicable also to thick disk accretion. Based on this consideration, we assume that even after the accreting star is spun up close to the Keplerian velocity at the surface, the star accretes matter at the initial rate while the surface velocity remains equal to the Keplerian velocity. We note that under this assumption the total angular momentum of the accreting white dwarf can even decrease.

Recently, Yoon & Langer (2004) computed white-dwarf models accreting CO-rich matter, taking into account the effect of rotation. The accretion rates they considered are lower than those adopted in our calculations. Their assumption at the surface of the accreting white dwarf is somewhat different from ours. They assumed that the matter accretes onto the white dwarf without bringing angular momentum when the rotation velocity at the surface of the white dwarf exceeds the Keplerian velocity. Under their assumption the total angular momentum of the white dwarf never decreases and is higher than that of our models for a given mass.

2. Models

The initial models, carbon-oxygen white dwarfs of $0.8M_\odot$ and $1M_\odot$, were obtained from zero-age helium main-sequence models by artificially suppressing nuclear reactions and converting chemical compositions to $(X_{\rm C}, X_{\rm O}, X_{\rm h}) = (0.48, 0.50, 0.02)$, where $X_{\rm h}$ denotes the mass fraction of the elements heavier than oxygen, and by letting cool until the central temperature became $\sim 10^7$K. Table 1 lists physical characteristics of the initial models. Adopted input physics are mostly the same as those used in Saio & Nomoto(1998): OPAL opacity tables (Iglesias & Rogers 1996), neutrino emission rates by Itoh et al. (1989), and carbon-burning reaction rates by Caughlan & Fowler (1988).

Keeping our evolutionary models spherical symmetric, we have included the effect of rotation only in the equation of hydrostatic equilibrium as

$$\frac{1}{\rho}\frac{dP}{dr} = -\frac{GM_r}{r^2} + \frac{2}{3}r\Omega^2, \tag{1}$$

where Ω is the angular velocity of rotation. The factor 2/3 comes from taking the mean of the radial component of the centrifugal force on a sphere (Kippenhahn et al. 1970). Spatial and time variation of Ω is determined by solving the conservation equation of angular momentum

$$\left[\frac{\partial(r^2\Omega)}{\partial t}\right]_{M_r} = \frac{\partial}{\partial M_r}\left[(4\pi\rho r^3)^2\nu\frac{\partial\Omega}{\partial M_r}\right], \tag{2}$$

where ν stands for turbulent viscosity. The outer boundary condition $\Omega = \Omega_{\rm K}$ was imposed at the photosphere, where $\Omega_{\rm K} = \sqrt{GM/R^3}$ is the Keplerian angular velocity at the stellar radius R. We have neglected the rotation of the initial models.

We have adopted two kinds of formulas for the turbulent viscosity; one from Fujimoto (1993) and another from Zahn (1992). The turbulent viscosity formulated by Fujimoto (1993) includes the effect of baroclinic instability as well as shear instability. We will refer this case as case A; the viscosity is given by

$$\nu_{\rm A} = \nu_{\rm KH} + \nu_{\rm BC}, \tag{3}$$

where

$$\nu_{\rm KH} = \begin{cases} \dfrac{1}{2Ri^{1/2}}(1-4Ri)^{1/2}H_p^2 N & \text{for} \quad Ri < 1/4 \\ 0 & \text{for} \quad Ri \geq 1/4; \end{cases} \tag{4}$$

$$\nu_{\rm BC} = \begin{cases} \dfrac{1}{3Ri^{1/2}}H_p^2\Omega & \text{for} \quad Ri \leq Ri_{\rm BC} \\ \dfrac{1}{3Ri^{3/2}}H_p^2\Omega & \text{for} \quad Ri > Ri_{\rm BC}, \end{cases} \tag{5}$$

$$Ri = N^2\left(\frac{d\Omega}{d\ln r}\right)^{-2}, \qquad Ri_{\rm BC} = 4\left(\frac{r}{H_p}\right)^2\frac{\Omega^2}{N^2} \tag{6}$$

with N being Brunt-Väisälä frequency defined as $N^2 = g(\Gamma_1^{-1}d\ln P/dr - d\ln\rho/dr)$ and H_p the pressure scale height.

For the second case, which is referred to as case B, we have included turbulent viscosity due to vertical shear instability formulated by Zahn (1992) but neglected the effect of meridional circulation; we have used the following equation,

$$\nu_{\rm B} = \frac{2}{45}\frac{K}{N^2}\left(\frac{d\Omega}{d\ln r}\right)^2, \tag{7}$$

where K is the thermal diffusivity defined by $K = 4acT^3/(3\kappa\rho^2 C_p)$. As we will see in the next section, the viscosity in case A is so efficient in transporting the angular momentum that the rotation becomes nearly uniform in the white-dwarf interior. In case B, on the other hand, the angular momentum is slowly transported into the deep interior. We assume that the two models for the transport of angular momentum bracket what occurs in a real star.

3. Numerical Results

Figure 1 shows the evolution of radius as a function of the total mass for C-O white-dwarfs that accrete CO-rich matter at rates of 10^{-5} and $5 \times 10^{-6} M_\odot \mathrm{y}^{-1}$ from the beginning of accretion to the off-center carbon ignition. The initial mass of the models is $1M_\odot$. Wiggles seen in this figure are numerical artifacts. The dotted lines show the evolution of non-rotating models, the solid lines for rotating models in case A, and the dashed lines for rotating models in case B.

In the early phase of accretion the radius of the white dwarf increases rapidly. This is caused by the fact that its envelope is heated by the accretion, and the centrifugal force of rotation lifts the envelope. The initial rapid expansion in case A models slows down when the angular momentum begins to be transferred back to the accretion disk (Fig.6 below). Such transition to a slower evolution did not occur in the models of Piersanti et al. (2003b), because they did not consider the possibility of transferring the angular momentum back to the disk, but did reduce the accretion rate. In later phase of accretion, the radius begins to decrease. The decrease in radius is caused by the increase of the white-dwarf mass. During this phase the total angular momentum is nearly constant or increases gradually. The lifting effect of rotation makes the radius of a rotating model larger than that of the non-rotating model with the same mass and the accretion rate.

A short vertical increase in radius at the end of each evolution track indicates the occurrence of the off-center carbon ignition. For a given accretion rate, the off-center carbon ignition occurs later in a rotating model than in the non-rotating model; i.e., the mass of the rotating white dwarf at the carbon ignition is larger than that for the corresponding non-rotating model.

Figure 2 shows the temperature versus M_r in the interior of models close to the off-center carbon ignition. These models have evolved from the initial model of $1M_\odot$ with an accretion rate of $10^{-5} M_\odot \mathrm{y}^{-1}$. The solid and dashed lines are for rotating models, and the dotted line for the non-rotating model. The outer layers consisting of accreted matter ($M_r > 1M_\odot$) have high temperatures heated by the gravitational energy release. The heat is conducted

into the layers of the original white dwarf. The heat-conduction front, however, has not advanced much during the time between the start of accretion and the off-center ignition ($\sim 10^4$y). Rotating models have broader temperature peaks than the non-rotating model, because they accrete more mass and hence the time from the start of accretion to the carbon ignition is longer. The core temperature has increased from the initial value $\log T = 7.08$ due to compression.

Table 2 lists the total mass $M_{\rm ig}$ and the central density $\rho_{\rm c}$ of the model in which off-center carbon-ignition occurs, and the mass interior to the ignition layer M_r(ig) for each case computed, where the values of masses are given in units of $M_\odot$, $\dot{M}$ means accretion rate in units of $M_\odot {\rm y}^{-1}$, and $M_{\rm i}$ stands for the initial mass. The difference in $M_{\rm ig}$ between a rotating and the non-rotating model for a given accretion rate can be as large as $\sim 0.1 M_\odot$. The value of M_r(ig) is also larger in the rotating model. Rotation delays the carbon ignition because the centrifugal force reduces the effective gravity to lift the outer layers and reduce the temperature there (Piersanti et al. 2003a). The lifting effect of rotation appears also in the central density, ρ_c, which is lower in the rotating model than in the non-rotating model with a similar mass. The case A models with $\dot{M} = 3 \times 10^{-6} M_\odot {\rm y}^{-1}$ did not ignite carbon. They began to expand before the maximum temperature in the outer layer reaches to the ignition temperature.

Table 2 shows that the results hardly depend on the initial mass of the white dwarf. The results confirm essentially the conclusion of the previous work done without including the effect of rotation that carbon is ignited in the outer layer of a C-O white dwarf if the accretion rate is fast enough.

4. Discussion

Figure 3 shows runs of the ratio of angular velocity to its local critical value, $\Omega/\Omega_{{\rm K},r}$, in the models at evolutionary stages around the carbon ignition for $\dot{M} = 10^{-5}$, 5×10^{-6} and $3 \times 10^{-6} M_\odot {\rm y}^{-1}$. (For the case A of $\dot{M} = 3 \times 10^{-6} M_\odot {\rm y}^{-1}$, $\Omega/\Omega_{{\rm K},r}$ in the last model computed is shown.) Here $\Omega_{{\rm K},r} = \sqrt{GM_r/r^3}$ is the local Keplerian velocity. In all cases, $\Omega/\Omega_{{\rm K},r}$ increases rapidly toward the surface in the very superficial layer, which is due to a rapid increase in the radius of mass shell toward the surface. In case A the viscous transport of angular momentum is very efficient so that the rotation becomes nearly uniform (Figs. 4,5). Therefore, the solid curves in Figure 3 are almost parallel to the runs of $r^{3/2} M_r^{-1/2}$. An exception is the outermost layer of the case A model for $\dot{M} = 3 \times 10^{-6} M_\odot {\rm y}^{-1}$. Since the radius of the model is rapidly increasing and hence the surface angular velocity (= Keplerian velocity) is rapidly decreasing, there is a steep outward decrease in the angular velocity of

rotation in the outermost layer (Fig.4 below).

In case B the angular momentum is hardly transported into the original white dwarf ($M_r \leq 1M_\odot$). Thus, the angular velocity at $M_r \sim 1M_\odot$ in the case B model of $\dot{M} = 10^{-5}M_\odot \mathrm{y}^{-1}$ is considerably larger than in the corresponding case A model. This account for the result that $M_{\rm ig}$ and M_r(ig) in case B with $\dot{M} = 10^{-5}M_\odot \mathrm{y}^{-1}$ are slightly larger than those for case A. In other cases, however, the effect of rotation is generally stronger in case A models than in case B models.

Figure 4 shows runs of angular velocity of rotation $\Omega(M_r)$ in the interior of models at selected phases of evolution for $\dot{M} = 3 \times 10^{-6}M_\odot \mathrm{y}^{-1}$ ($M_{\rm i} = 1M_\odot$). Figure 5 shows the same information for $\dot{M} = 1\times10^{-5}$ (lower panel) and $5\times10^{-6}M_\odot \mathrm{y}^{-1}$ (upper panel). Obviously, the angular momentum transport by the turbulent viscosity in case A is so efficient that $\Omega(M_r)$ is nearly constant in the interior. In the case A model with $\dot{M} = 3 \times 10^{-6}M_\odot \mathrm{y}^{-1}$, $\Omega(M_r)$ varies steeply in the very superficial layer when the total mass is larger than $1.35M_\odot$ (Fig. 4). Since Ω at the stellar surface is always set to be the critical frequency Ω_K ($\propto M^{1/2}R^{3/2}$), a steep increase in $\Omega(M_r)$ toward the surface indicates the star is rapidly contracting, and a steep decrease indicates a rapid expansion. The surface angular velocity changes so rapidly that the transport of angular momentum is not efficient enough to keep the angular velocity of rotation in the interior close to the surface value. The model contracts first and then expands rapidly.

In the interior of a case B model there is a peak in $\Omega(M_r)$, which is produced by compression. The angular velocity at the peak is higher than that at the surface of the model. Although Ω decreases steeply outward near the surface, the specific angular momentum $r^2\Omega$ increases outward there because the distance from the center of a mass shell increases outward steeply near the surface. In early phases of accretion, there is a narrow layer where the specific angular momentum decreases outward just outside of the peak in Ω at $M_r \sim 1.0M_\odot$. But, the structure is always stable to the Solberg-Høiland instability, because the temperature gradient is positive there and hence the stabilizing effect of buoyancy exceeds the destabilizing effect of the negative gradient of the specific angular momentum distribution.

Figure 6 shows the evolution of the total angular momentum of the models accreting matter at $\dot{M} = 10^{-5}$, 5×10^{-6} and $3 \times 10^{-6}M_\odot \mathrm{y}^{-1}$. The higher the accretion rate, the lower the total angular momentum at a given total mass. In case A models (solid lines) the total angular momentum, J, increases rapidly until a mass of $\approx 0.01M_\odot$ is accreted. After the total angular momentum attains a peak, (when the angular velocity in the interior becomes almost constant), it decreases as the total mass increases to $\approx 1.1M_\odot$, returning part of the accumulated angular momentum to the disk. For $M \gtrsim 1.1M_\odot$, J increases but very slowly. In this phase most of the angular momentum associated with the accreted matter is returned

to the disk.

To compare the evolutionary $M - J$ relations with those of simpler models, we have computed uniformly and critically rotating steady models, in which the rate of entropy change $(\partial s/\partial t)_{M_r}$ is replaced with $-(\partial s/\partial \ln q)_t \dot{M}/M$ where $q = M_r/M$ (e.g., Kawai et al. (1987)), and the nuclear reactions are artificially suppressed. The $M - J$ relation of the steady model for each accretion rate is shown by a dash-dotted line in Fig 6. (Detailed properties of the steady models will be presented in a future paper.) This figure shows that the gradual increase of J with a increase in mass in the range $M \gtrsim 1.1 M_\odot$ occurs along the $M - J$ relation of the steady model with the same accretion rate, indicating the evolution in this phase occurs nearly homologously.

The total angular momentum in a case B model is smaller than the case A model with the same mass and accretion rate. Since the angular momentum transport in the case B models is less efficient then in the case A models, more angular momentum is returned to the accretion disk in the former case.

The total angular momentum of a case A model is smaller than that of the uniformly and critically rotating white dwarf of the same mass without accretion (Uenishi, Nomoto, Hachisu 2003). The difference is attributed to the fact that the critical angular velocity of rotation for the the accreting white dwarf is lower than that of the white dwarf without accretion, because the radius of the former is larger.

When the mass of the white dwarf becomes larger than $\sim 1.36 M_\odot$, the total angular momentum J of the case A model of $\dot{M} = 3 \times 10^{-6} M_\odot \mathrm{y}^{-1}$ begins to decrease due to a rapid decrease in radius. The commencement of the rapid contraction roughly corresponds to the phase when the mass of the white dwarf exceeds the maximum mass of the steady model for the same accretion rate. At $M \approx 1.39 M_\odot$ the radius and the total angular momentum become minimum and carbon burning is almost ignited at $M_r = 1.38 M_\odot$. However, at this point the model begins to expand and the total angular momentum begins to increase. Due to the expansion, the maximum temperature in the interior decreases, and carbon ignition does not occur in this model. Further computation became too difficult to continue. We note however that if the viscosity is switched to the case B viscosity, we can continue the calculation to have a massive (say $2 M_\odot$) model having a high angular momentum, in which $\Omega(M_r)$ has a broad peak similar to those shown in Yoon & Langer (2004).

Finally, we note that the ratio of the rotational kinetic energy to the absolute value of the gravitational potential energy defined as

$$\frac{T}{|W|} = \frac{1}{2} \int_0^M r^2 \Omega^2 dM_r \left[\int_0^M \frac{G M_r}{r} dM_r \right]^{-1} \tag{8}$$

is always less than 0.03 in our models. For such a small ratio, no dynamical instability occurs unless a very strong differential rotation in the deep interior of the star exists (Shibata et al. 2003). The ratios $T/|W|$ of our models are smaller than the corresponding ratio denoted by γ in Piersanti et al. (2003b) for the critically rotating model with a similar accretion rate, where γ is defined as

$$\gamma = \frac{1}{2}\int_0^M r^2\Omega^2 dM_r \left[\frac{1}{2}\frac{GM^2}{R}\right]^{-1}. \quad (9)$$

A rotating and accreting white dwarf has a large radius because the outer envelope (in which only a small fraction of mass resides) is expanded, while the inner layers contribute to the gravitational energy. Therefore, $|W|$ is generally larger than $\frac{1}{2}GM^2/R$ for the rotating and accreting models. In fact, $|W|$ of our models can be as large as $1.6 \times GM^2/R$, which makes $T/|W|$ as small as $\gamma/3$. Even if γ defined by equation (9) reached 0.14, $T/|W|$ can be as small as ~ 0.05. Since $T/|W|$ should be used for the stability criterion rather than γ, our models should be stable. We also note that the $T/|W|$ ratios of the models in Yoon & Langer (2004) are larger than those of our models. This is attributed to the fact that in the interior of their models there exist a broad peak of the angular velocity.

5. Conclusion

Taking into account the centrifugal force of rotation, we computed models of CO-white dwarfs that accrete CO-rich matter up to the carbon-ignition. We assumed that the surface angular velocity of rotation is equal to the Keplerian angular velocity. We have found that carbon is ignited in an outer layer if the accretion rate is greater than $3 \times 10^{-6} M_\odot \mathrm{y}^{-1}$. The rotation delays the ignition. The difference in the total mass at the ignition between rotating and non-rotating models can be as large as $\sim 0.1 M_\odot$, depending on the assumed turbulent viscosity and the accretion rate (see Uenishi et al. (2003) for the 2D models).

When the double white dwarfs coalesce, the more massive white dwarf is expected to accrete CO-rich matter at a rate close to the Eddington limit ($\sim 10^{-5} M_\odot \mathrm{yr}^{-1}$). We have found in this paper that such a high accretion rate leads to an off-center carbon ignition even if the effect of rapid rotation is included. Once the ignition occurs, the carbon flame propagates through the interior to the stellar center due to conduction and the C-O white dwarf is converted to an O-Ne-Mg white dwarf peacefully (Saio & Nomoto 1985, 1998; Timmes et al. 1994). The result of our computation including the effect of rotation supports our previous conclusion that a double C-O white dwarf merger would *not* yield a SN Ia.

We are grateful to the referee for the constructive comments. This work has been

supported in part by the grant-in-Aid for COE Scientific Research (15204010, 16042201, 16540229) of the Ministry of Education, Culture, Science, Sports, and Technology in Japan.

REFERENCES

Benz, W., Cameron, A.G.W., Press, W.H., & Bowers, R.L., 1990, ApJ, 348, 647

Caughlan, G.R. & Fowler, W.A. 1988, Atomic data Nuclear data tables 40, 283

Fujimoto, M.Y. 1993, ApJ, 419, 768

Fujimoto, M.Y. 1995, ApJ, 450, 262

Iben, I.Jr., & Tutukov, A.V., 1984, ApJS, 54, 335

Iglesias, C.A., & Rogers, F.J. 1996, ApJ, 464, 943

Itoh, N., Adachi, T., Nakagawa, M., Koyama, Y., & Munakata, H. 1988, ApJ, 339, 354

Kawai, S., Saio, H., & Nomoto, K. 1987, ApJ, 315, 229

Kippenhahn, R., Meyer-Hofmeister, E., & Thomas, H.C. 1970, A&A, 5, 155

Mochkovitch, R., & Livio, M. 1990, A&A, 236, 378

Nomoto, K. 1984, ApJ, 277, 791

Nomoto, K. 1987, ApJ, 322, 206

Nomoto, K., & Iben, I.,Jr. 1985, ApJ, 297, 531

Nomoto, K., & Kondo, Y. 1991, ApJ, 367, L19

Paczyński, B. 1991, ApJ, 370, 597

Piersanti, L., Gagliardi, S., Iben, I.Jr., & Tornambe, A. 2003a, ApJ, 583, 885

Piersanti, L., Gagliardi, S., Iben, I.Jr., & Tornambe, A. 2003b, ApJ, 598, 1229

Popham, R., & Narayan, P. 1991, ApJ, 370, 604

Rasio, F.A. & Shapiro, S.L., 1995, ApJ, 438, 887

Saio, H., & Nomoto, K. 1985, A&A, 150, L21

Saio, H., & Nomoto, K. 1998, ApJ, 500, 388

Shibata, M., Karino, S., & Eriguchi, Y. 2003, MNRAS, 343, 619

Timmes, F.X., Woosley, S.E., & Taam, R.E. 1994, ApJ, 420, 348

Uenishi, T., Nomoto, K., & Hachisu, I. 2003, ApJ, 595, 1094

Webbink, R.F. 1984, ApJ, 277, 355

Yoon, S.-C., & Langer, N. 2004, A&A, 419, 623

Zahn, J.-P. 1992, A&A, 265, 115

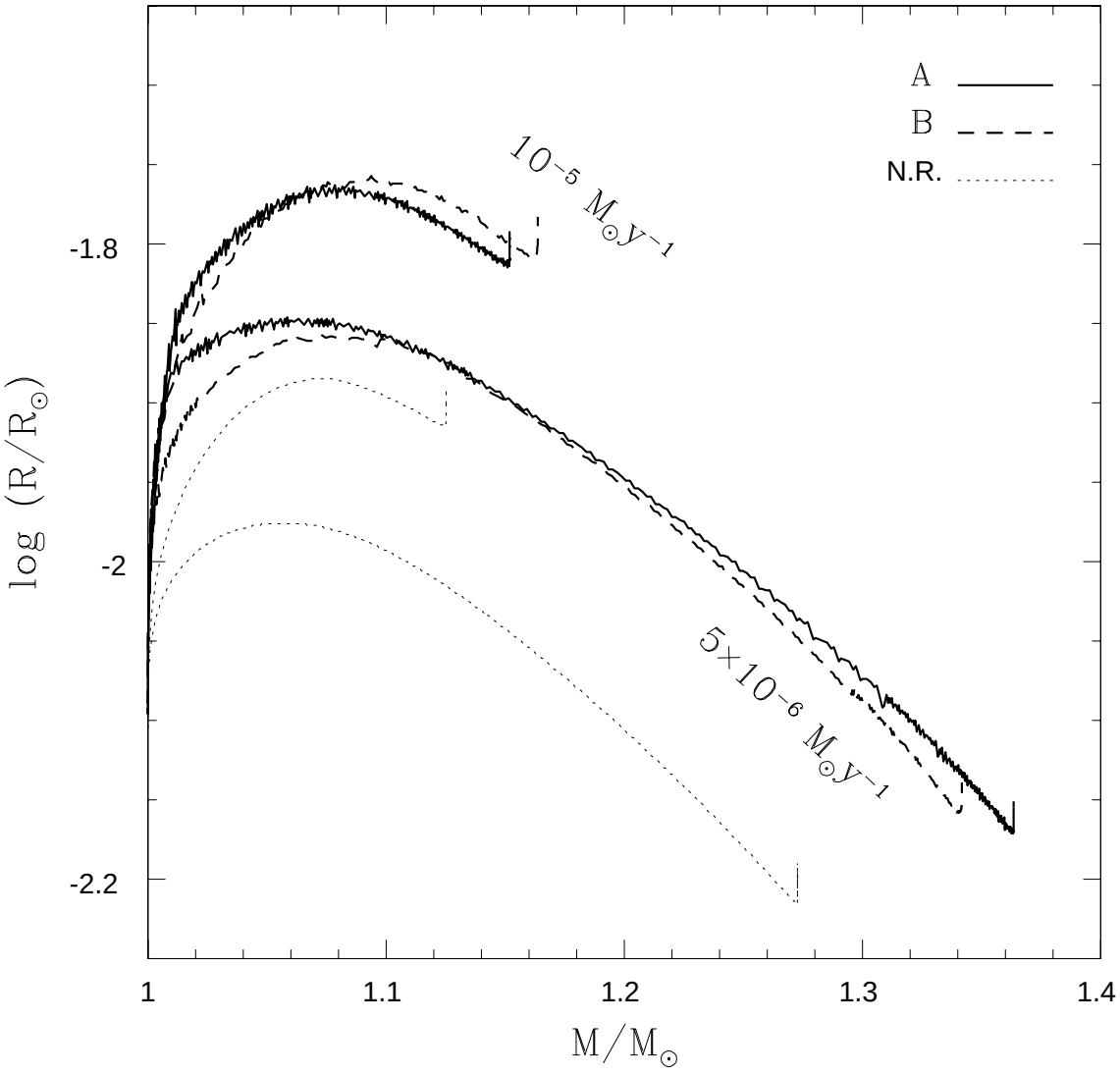

Fig. 1.— Evolution of C-O white dwarfs that accrete CO-rich matter at rates of 10^{-5} and $5 \times 10^{-6} M_\odot \mathrm{y}^{-1}$. The ordinate and the abscissa are, respectively, the radius and the mass of the white dwarf. The solid (case A) and dashed (case B) lines are for rotating models in which the angular momentum transport is calculated using relatively high (A) and low (B) turbulent viscosities, respectively. The dotted lines are for non-rotating models. The nearly vertical increase in radius at the end of each evolution indicates the occurrence of an off-center carbon ignition.

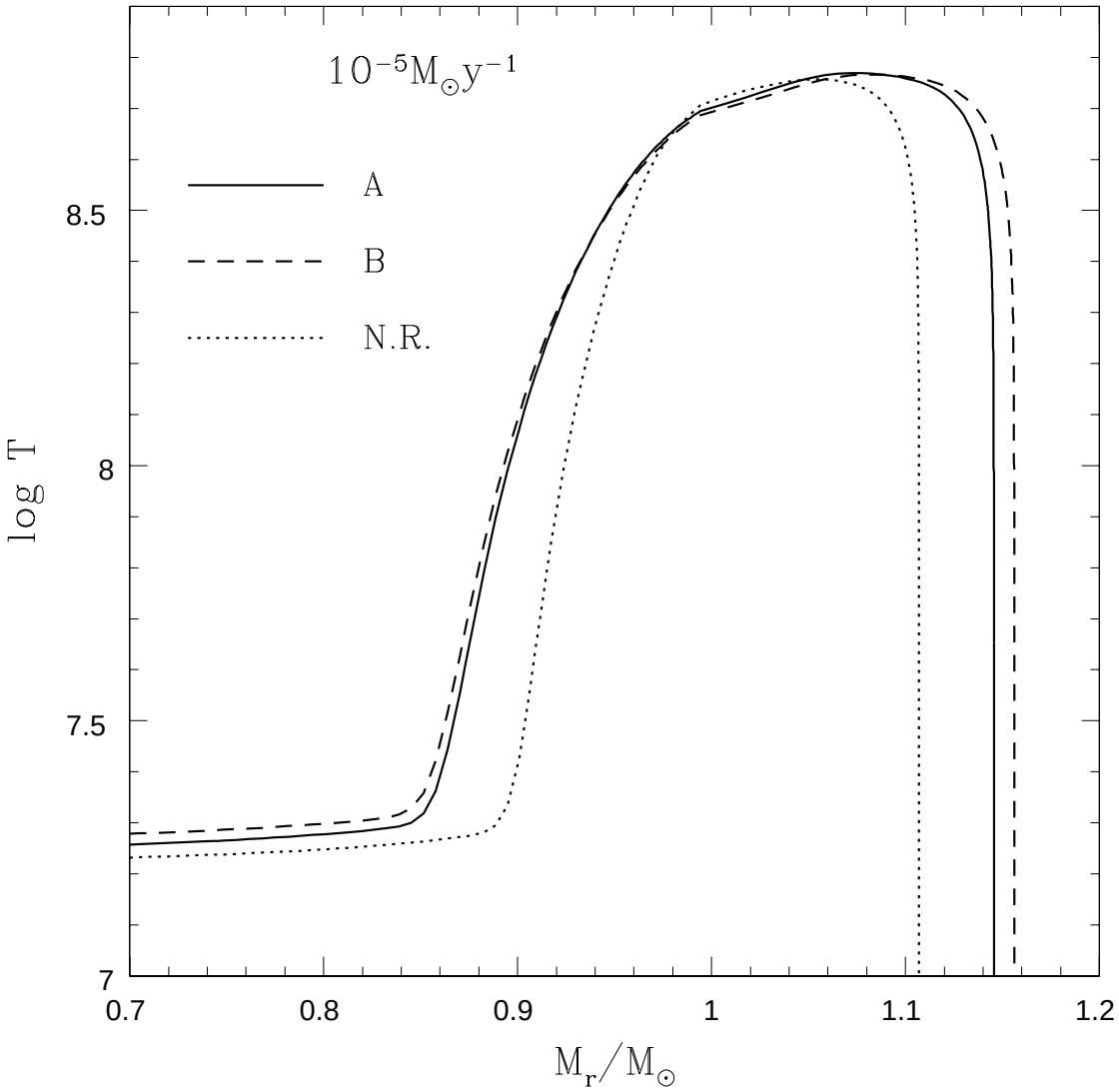

Fig. 2.— Temperature distributions in models close to the off-center carbon ignition for an accreting rate of $10^{-5}M_\odot y^{-1}$. The solid and the dashed line are for rotating models with different turbulent viscosities. The dotted line is for the non-rotating model.

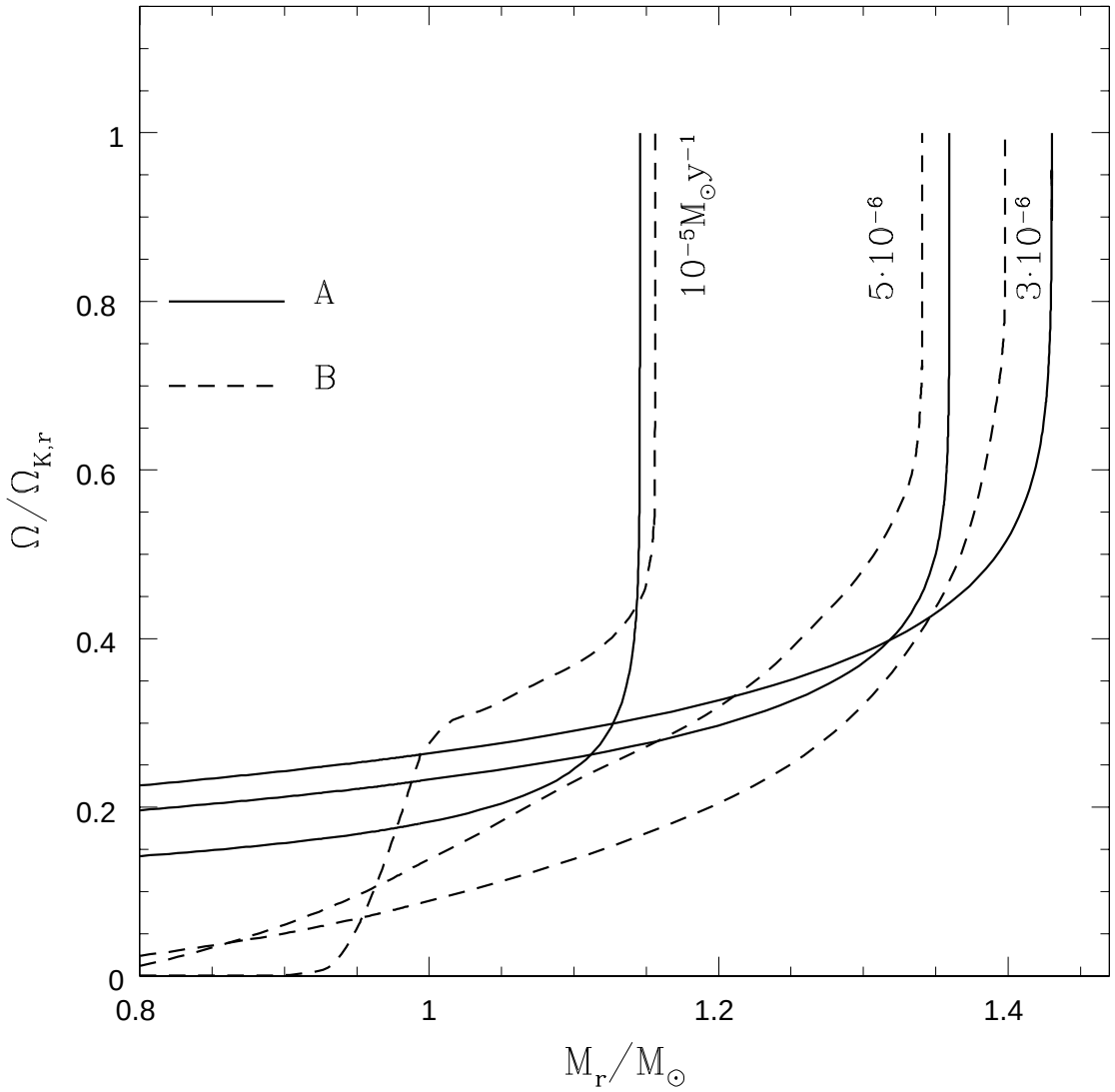

Fig. 3.— Runs of the ratio of angular velocity of rotation to the local Keplerian frequency, $\Omega_{\mathrm{K},r}$, in the interior of models for accretion rates of 10^{-5}, 5×10^{-6}, and $3\times10^{-6}M_\odot\mathrm{y}^{-1}$. The abscissa represents the mass coordinate in units of solar mass.

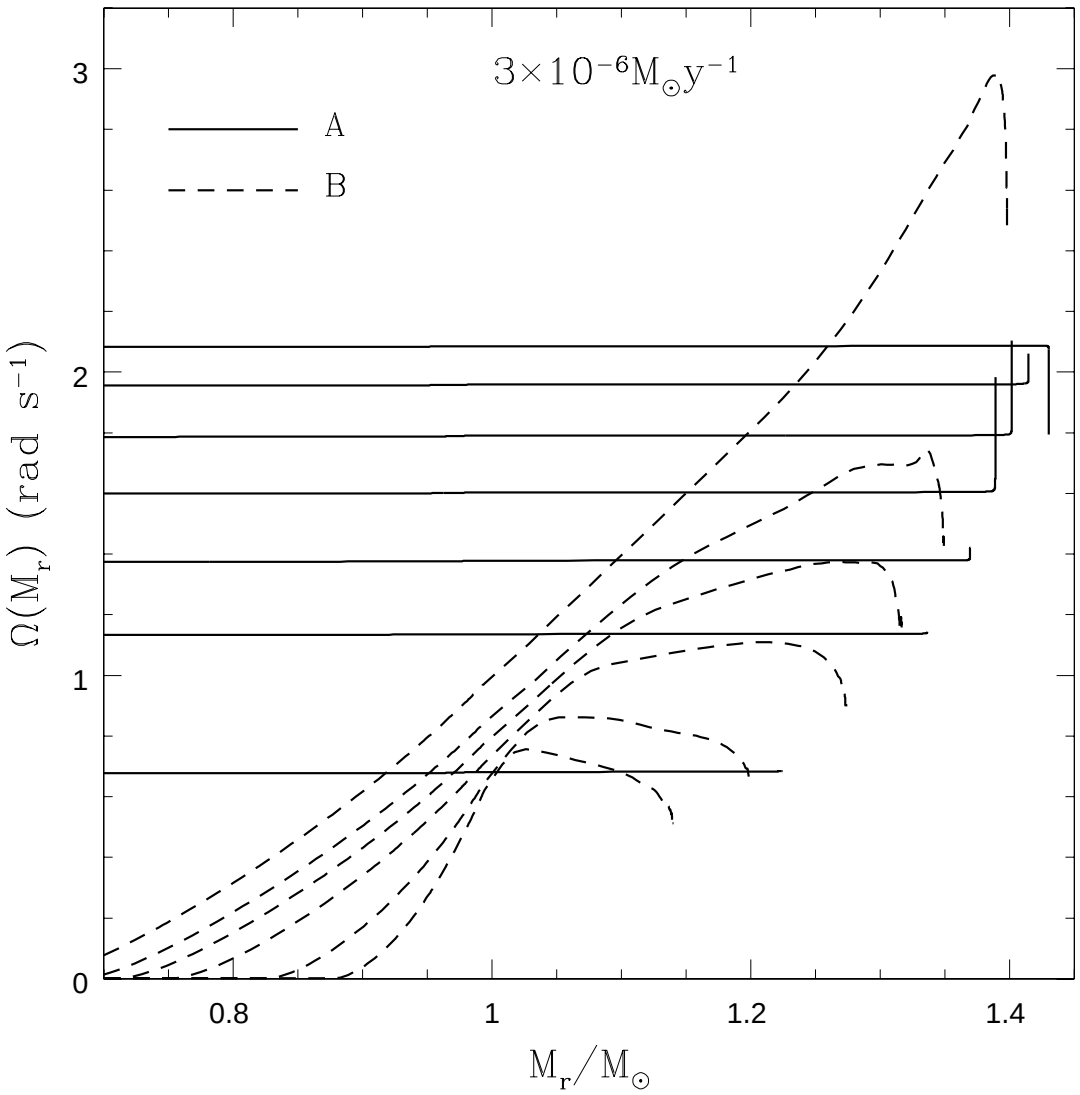

Fig. 4.— Runs of angular velocity of rotation, $\Omega(M_r)$, in the interior of models at selected evolutionary stages for the accretion rate $\dot{M} = 3 \times 10^{-6} M_\odot \mathrm{y}^{-1}$.

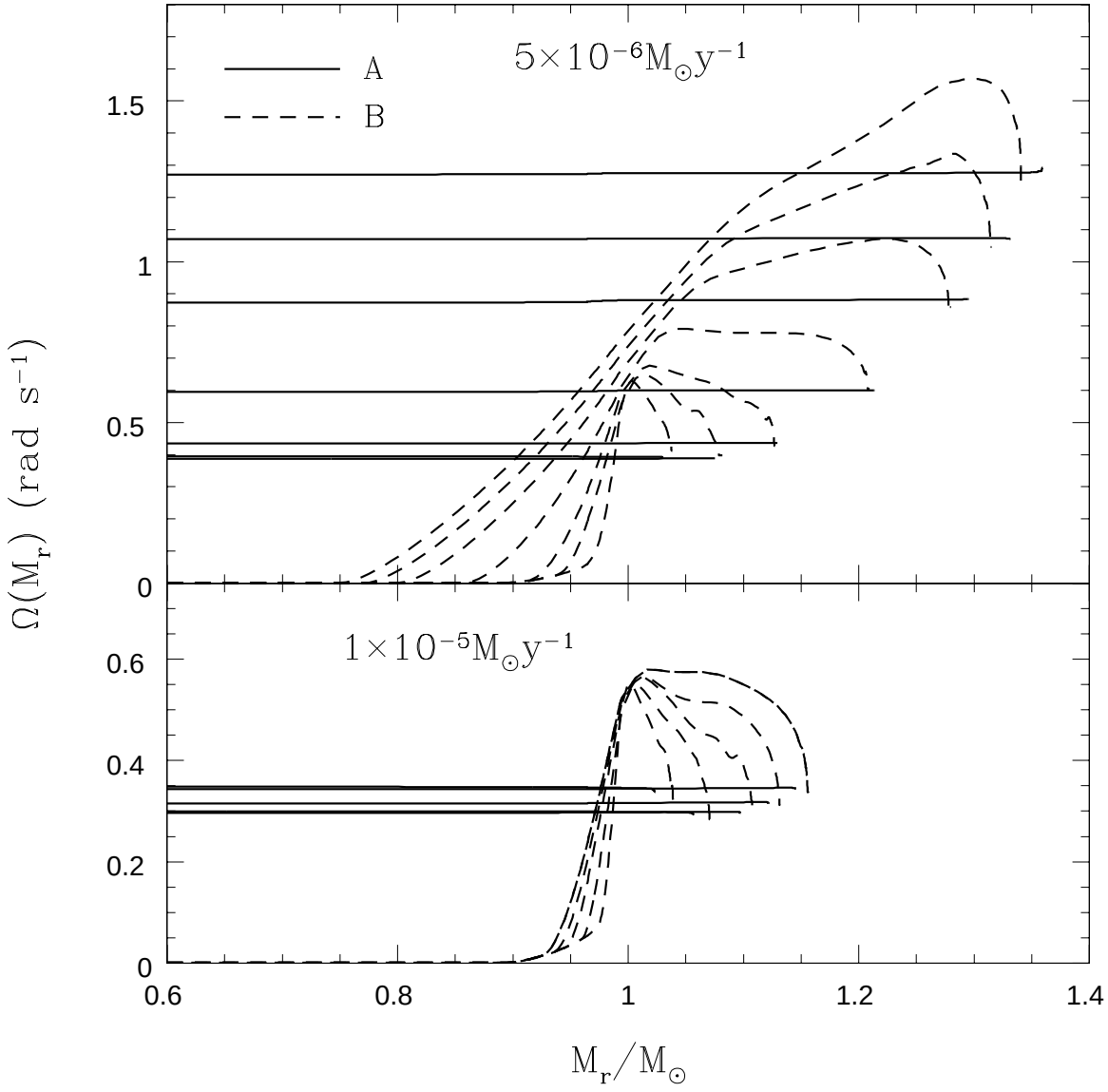

Fig. 5.— The same as Fig. 4 but for for $\dot{M} = 10^{-5}$ (lower panel) and $5 \times 10^{-6} M_\odot \mathrm{y}^{-1}$ (upper panel).

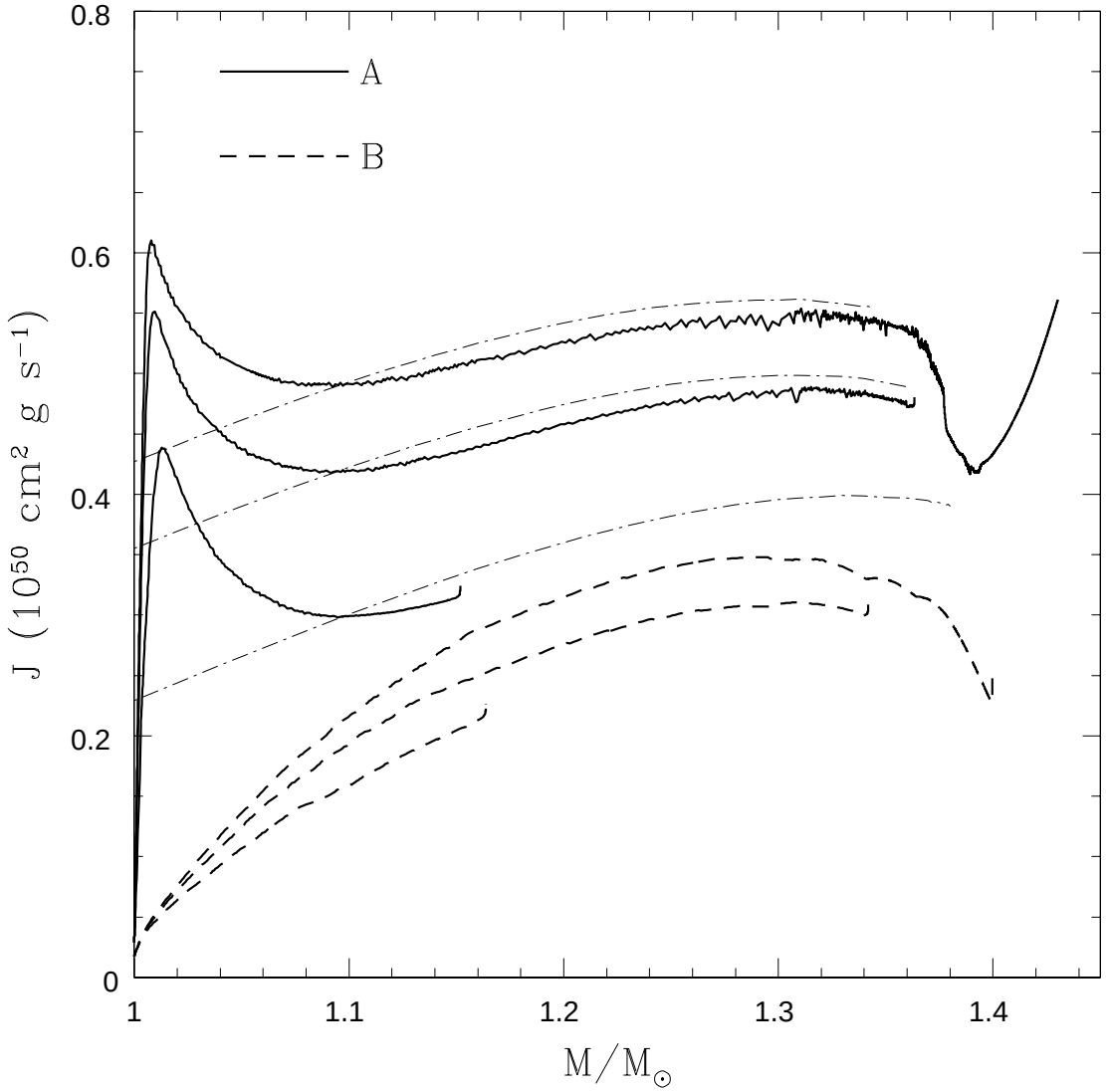

Fig. 6.— Evolution of the total angular momentum J of C-O white dwarfs with respect to the total mass for accretion rates of 3×10^{-6}, 5×10^{-6}, and $10^{-5} M_{\odot}\mathrm{y}^{-1}$. The lower the accretion rate, the higher is the total angular momentum for a given total mass. Dash-dotted lines show the relations of uniformly and critically rotating steady models for those mass-accretion rates.

Table 1. Physical characteristics of initial models

$M/M_\odot$	$\log T_{\rm c}$	$\log \rho_{\rm c}$	$\log L/L_\odot$	$\log R/R_\odot$
0.8	7.086	7.024	−2.286	−1.999
1.0	7.081	7.528	−2.216	−2.105

Table 2. Summary of numerical results

		No rot.			Rot. A			Rot. B		
$\dot{M}$	$M_{\rm i}$	M_r(ig)	$M_{\rm ig}$	$\log \rho_{\rm c}$	M_r(ig)	$M_{\rm ig}$	$\log \rho_{\rm c}$	M_r(ig)	$M_{\rm ig}$	$\log \rho_{\rm c}$
3×10^{-6}	1.0	1.35	1.36	9.15	–	–	–	1.38	1.40	9.25
3×10^{-6}	0.8	1.35	1.36	9.13	–	–	–	1.39	1.40	9.24
5×10^{-6}	1.0	1.24	1.27	8.47	1.33	1.36	8.64	1.31	1.34	8.67
5×10^{-6}	0.8	1.25	1.28	8.48	1.33	1.37	8.64	1.31	1.35	8.66
1×10^{-5}	1.0	1.05	1.12	7.82	1.07	1.15	7.83	1.08	1.16	7.87
1×10^{-5}	0.8	0.98	1.09	7.65	1.01	1.13	7.70	1.02	1.14	7.72